

Airy pulse shaping using time-dependent power-law potentials

Tianwen Han,¹ Hao Chen,¹ Chengzhi Qin,¹ Wenwan Li,¹ Bing Wang,^{1,*} and Peixiang Lu^{1,2,†}

¹Wuhan National Laboratory for Optoelectronics and School of Physics, Huazhong University of Science and Technology, Wuhan 430074, China

²Laboratory for Optical Information Technology, Wuhan Institute of Technology, Wuhan 430205, China



(Received 2 March 2018; revised manuscript received 19 April 2018; published 8 June 2018)

We investigate the temporal and spectral evolutions of finite-energy Airy pulses in the presence of power-law optical potentials. The potentials are generated by the time-dependent pumped light, which propagates together with the Airy pulses in a highly nonlinear optical fiber. We show that the intrinsic acceleration of Airy pulses can be modified by an external force that stems from a linear potential, and hence unidirectional frequency shift can be realized. When a triangle potential is employed, the pulse will exhibit self-splitting both in temporal and spectral domains. Additionally, as a parabolic potential is utilized, both the temporal waveform and frequency spectrum of the Airy pulse will exchange alternately between the Airy and Gaussian profiles. By using higher-order power-law potentials, we also realize both revival and antirevival effects for the Airy pulses. The study may find wide applications in pulse reshaping and spectral-temporal imaging for both optical communication and signal processing.

DOI: [10.1103/PhysRevA.97.063815](https://doi.org/10.1103/PhysRevA.97.063815)

I. INTRODUCTION

In 1979, Berry and Balazs [1] found that the nonspreading Airy wave packet could be a solution of the free particle Schrödinger equation, which has the form of the Airy function. The most prominent feature of the Airy wave packet is the self-accelerating behavior without external force. However, this wave packet contains infinite energy and cannot be realized physically. Siviloglou and Christodoulides and co-workers firstly proposed theoretically [2] and experimentally demonstrated [3] the concept of the finite-energy Airy beams (FEABs) with limited beam width. The FEABs have attracted considerable interest due to the intriguing characteristics including transverse self-accelerating [4], diffraction-free propagating [5], and self-healing [2,6]. These features have found wide applications in particle trapping [7,8], light bullets [9,10], curved surface plasma [11,12], and nonlinear optical effects [13–19]. Additionally, the propagation of FEABs can be controlled through external optical potentials, realized by tailoring the transverse refractive index distribution of the medium [20–25].

Recently, inspired by the time-space duality [26], the temporal finite-energy Airy pulses (FEAPs) have also been proposed by exploiting the analogy between spatial paraxial diffraction and temporal narrow-band dispersion. The FEAPs can be obtained as a Gaussian pulse propagates through a third-order dispersion fiber [27] or by imparting cubic phase modulation onto a Gaussian pulse [28]. Analogously, FEAPs manifest the characteristics of dispersion-free propagating [29], self-accelerating, and self-healing, which have been used in supercontinuum generation [30] and signal frequency shifting [31–33]. Recently, it has been reported that the propagation of FEAPs can be controlled by dispersion modulation

[34,35], initial frequency chirping [36], and Kerr nonlinearities [37,38]. In fact, a temporal potential generated by the nonlinear interaction between weak signal and strong pump lasers can be used for either temporal or spectral signal manipulation [39–42]. In quantum systems, the power-law potentials have been intensively investigated since the linear potential could arouse acceleration of particles and the parabolic potential is often associated with harmonic oscillation. Additionally, the higher-order potentials usually lead to nonlinear light-matter interaction. It has been reported that a time-dependent wave packet may exhibit revival behavior in a one-dimensional power-law potential [43].

In this work, we shall study the temporal-spectral dynamics of FEAPs in time-varying optical potentials including linear, parabolic, and higher-order power-law potentials. We show that within a linear potential, the Airy pulse acceleration can be enhanced or reduced, and the frequency spectrum unidirectional shift can be realized accordingly. When a triangle potential is utilized, the pulse will experience self-splitting both in temporal and spectral domains. Interestingly, as a parabolic potential is employed, the temporal profile and spectrum envelope of the Airy pulse will both alternately change between the Airy and Gaussian shapes. We also analyze the pulse center and widths variation during propagation. In addition, the revival and antirevival behaviors of the Airy pulse are observed for higher-order potentials. The revival distance decreases as the order increases. The study provides a promising approach to shape the temporal and spectral envelopes of an Airy pulse.

II. THEORETICAL MODEL

We consider a signal light of an Airy pulse propagating in a highly nonlinear optical fiber. In the presence of cross-phase modulation (XPM) between the weak signal light and a copropagating strong pump light, the pulse envelope can be

*wangbing@hust.edu.cn

†lupeixiang@hust.edu.cn

described by the modified nonlinear Schrödinger equation,

$$\frac{\partial A_s}{\partial z} + \beta_1 \frac{\partial A_s}{\partial t} + \frac{i\beta_2}{2} \frac{\partial^2 A_s}{\partial t^2} = i2\gamma |A_p|^2 A_s, \quad (1)$$

where A_s is the slowly varying amplitude of the signal light. A_p is the amplitude of the pump light, which is assumed to be constant during propagation. $\beta_1 = 1/v_g$ is the group delay with v_g being the pulse group velocity. β_2 is the second-order dispersion (GVD) coefficient and γ is the Kerr nonlinear coefficient for the fiber. Note that the higher-order dispersion and the self-phase modulation (SPM) effect are neglected here. It has been revealed that the third-order dispersion can realize inversion propagation and tight focusing for the Airy pulse [34]. Since we consider a long-duration Airy pulse, the effect of third-order dispersion is negligible with respect to that of GVD. For the SPM effect, it can lead to the soliton shedding effect for the Airy pulse [37,38]. However, due to the weak intensity of the signal light compared to the pumped light, the influence of SPM is much weaker than that of XPM and can be neglected. Additionally, the required optical potentials for the Airy pulse are created through XPM [39] by controlling the intensity profiles of the pumped light. Generally, Eq. (1) can be rewritten in the normalized form,

$$i \frac{\partial U}{\partial Z} + \left[\frac{1}{2} s \frac{\partial^2}{\partial T^2} + N^2 V(T) \right] U = 0, \quad (2)$$

where $U = A_s/A_0$; $V(T) = |A_p|^2/A_0^2$ denotes the normalized amplitudes of the signal and pump light with A_0 being the pulse peak amplitude. $T = (t - z/v_g)/T_0$ is the normalized time in the frame of reference moving at a group velocity of v_g . T_0 is an arbitrary time scale, which is usually chosen as the main lobe width of the Airy pulse. For $T > 0$, the Airy pulse is accelerating; otherwise, it is decelerating. $Z = z/L_{D2}$ represents the normalized propagation distance, which is measured in units of the dispersion length $L_{D2} = T_0^2/|\beta_2|$. $s = 1$ (or $s = -1$) denotes the anomalous or normal group velocity dispersion, respectively. Here we choose $s = 1$. $N^2 = 2L_{D2}/L_{NL}$; $L_{NL} = 1/(\gamma A_0^2)$ is the nonlinear length. In this work, we assume $N = 1$ with appropriate choices of L_{D2} and L_{NL} .

The envelope of the FEAPs can be described by $U(T) = \text{Ai}(T)\exp(aT)$, where $\text{Ai}(T) = \int_{-\infty}^{\infty} \exp(-i8\pi^3 v^3/3 - 2\pi i v T) dv$ is the Airy function with $a(0 < a < 1)$ being the truncation coefficient. In the absence of external potential, the Airy pulse exhibits self-acceleration in the T - Z plane along a parabolic temporal trajectory [35], as shown in Fig. 1(a). As the time-varying potential $V(T)$ interacts with the Airy pulse shown in Fig. 1(b), the propagation dynamics of the Airy pulse can be engineered. Due to the enormous degrees of freedom in choosing the format of the time-varying potentials, the Airy pulse can be tailored to exhibit various propagation properties. In this work, we investigate a family of power-law potentials, which are generally described by [43]

$$V_n(T) = V_0 |T|^n, \quad (3)$$

where V_0 is the effective potential depth. Specifically, the potential is linear for $n = 1$ and parabolic for $n = 2$. For

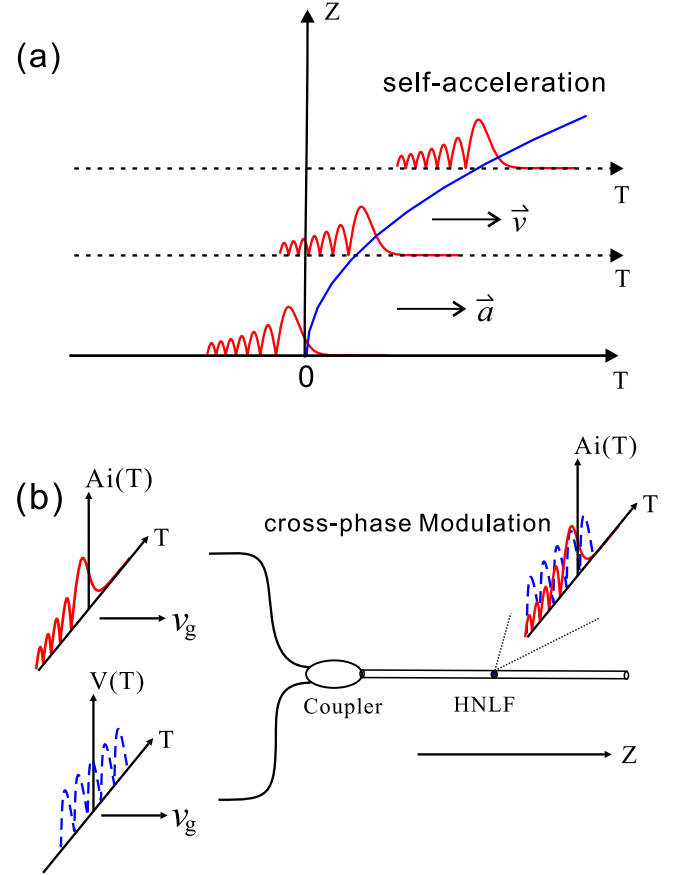


FIG. 1. (a) Schematic of self-acceleration of a finite-energy Airy pulse in normalized coordinates. (b) Schematic of the cross-phase interaction between the Airy pulse (red solid line) and the optical potential (blue dashed line) in a highly nonlinear fiber (HNLF). The potential is generated by a time-varying light field.

sufficiently large n , it will approach a potential well of infinite depth.

III. RESULTS AND DISCUSSION

A. Airy pulse propagation in linear potential

Firstly, we consider the linear temporal potential, which is given by

$$V(T) = \beta T, \quad (4)$$

where β is the gradient of the linear potential, which is equivalent to a constant force applied along the time coordinate. By performing Fourier transformation [44], we can obtain the evolution of the FEAPs:

$$\begin{aligned} U(T, Z) &= \text{Ai} \left[\left(T - \frac{Z^2}{4} + \frac{\beta Z^2}{2} \right) + iaZ \right] \\ &\times \exp \left(aT - \frac{a}{2} Z^2 + i \frac{a^2}{2} Z + i \frac{T}{2} Z - \frac{i}{12} Z^3 \right) \\ &\times \exp \left(\frac{a}{2} \beta Z^2 + \frac{i}{4} \beta Z^3 + i V_0 Z - i \beta T Z - \frac{i}{6} \beta^2 Z^3 \right). \end{aligned} \quad (5)$$

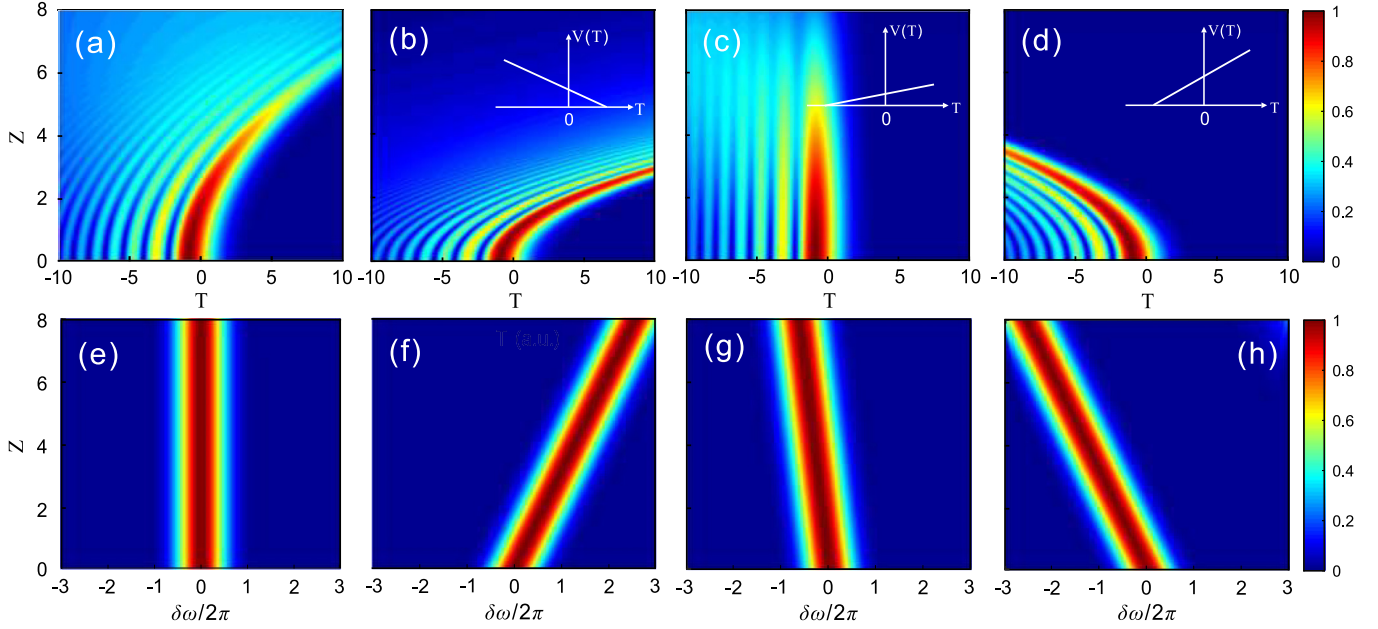


FIG. 2. (a)–(d) Temporal evolutions of a finite-energy Airy pulse in a linear potential with different gradient β : (a) $\beta = 0$. (b) $\beta = -2$. (c) $\beta = \frac{1}{2}$. (d) $\beta = 2$. (e)–(h) The corresponding spectral evolutions for the Airy pulse in (a)–(d). Other parameters are $a = 0.05$ and $T_0 = 100$ ps.

It shows that the Airy pulse propagates along a parabolic trajectory $T(Z) = (\frac{1}{4} - \beta/2)Z^2$ in the T - Z plane. The corresponding “velocity” and “acceleration” are $v = dT/dZ = (\frac{1}{2} - \beta)Z$ and $a = d^2T/dZ^2 = \frac{1}{2} - \beta$. Here $\frac{1}{2}$ is the intrinsic acceleration and $-\beta$ is the external acceleration imposed by the applied linear potential. For $\beta < 0$, the Airy pulse will be accelerated even faster. On the contrary, for $\beta > 0$, the acceleration will decrease. Specifically for $\beta = \frac{1}{2}$, the acceleration can be completely canceled. For $\beta > \frac{1}{2}$, the Airy pulse can be even accelerated in the opposite direction.

To confirm the above analysis, we simulate the Airy pulse propagation in linear potential by using the split-step Fourier method [26]. The simulation results are shown in Fig. 2. Figure 2(a) shows the temporal evolution of the Airy pulse without external potential, which exhibits the characteristic parabolic trajectory. For $\beta = -2$ shown in Fig. 2(b), the Airy pulse is accelerated even faster with larger deflection in the time dimension. Specifically for $\beta = \frac{1}{2}$ as shown in Fig. 2(c), the additional acceleration provided by the external potential can cancel the intrinsic acceleration. On the contrary, $\beta = 2$ will lead to the displacement of the Airy pulse in the opposite time dimension, as depicted in Fig. 2(d). The enhanced or reduced acceleration of the Airy pulse is valuable for many applications [4,12].

Next we investigate the influence of the linear potential on the spectral evolution of the Airy pulse. From Eq. (5), the instantaneous phase shift of $\Delta\varphi(T, Z) = -\beta TZ$ corresponds to the instantaneous frequency shift and chirp:

$$\begin{aligned} \delta\omega(Z) &= \frac{\partial\Delta\varphi(T, Z)}{\partial T} = -\beta Z, \\ c(Z) &= \frac{1}{2\pi} \frac{\partial^2\Delta\varphi(T, Z)}{\partial T^2} = 0. \end{aligned} \quad (6)$$

Therefore the linear potential can induce a linear spectral shift for the Airy pulse. Also note that the chirp vanishes, and

the spectrum can maintain its shape during the propagation process. The simulated spectral evolutions for $\beta = 0, -2, \frac{1}{2}$, and 2 are shown in Figs. 2(e)–2(h), which exhibit no spectral shift, linear blueshift, and linear redshift, respectively. Meanwhile, the spectral bandwidth can stay unchanged during propagation.

By combining two linear potentials, we can construct a symmetric triangle potential $V(T) = \beta|T|$. The solution of Eq. (2) can be written as

$$\begin{aligned} U(T, Z) &= \text{Ai} \left[\left(T - \frac{Z^2}{4} \mp \frac{\beta Z^2}{2} \right) + iaZ \right] \\ &\times \exp \left[a \left(T \mp \frac{a}{2} \beta Z^2 \right) - \frac{a}{2} Z^2 \right] \\ &\times \exp \left[\frac{i}{2} \left(a^2 + T \mp \frac{a}{2} \beta Z^2 \right) Z \right. \\ &\left. + i(\pm\beta TZ) - \frac{i}{6} \beta^2 Z^3 - \frac{i}{12} Z^3 \right], \end{aligned} \quad (7)$$

where we choose “+(-)” for $T > 0$ or $T < 0$. The corresponding temporal trajectory is thus given by

$$T = \frac{Z^2}{4} \pm \frac{\beta Z^2}{2}. \quad (8)$$

The “acceleration” is thus $\frac{1}{2} + \beta$ for $T < 0$ and $\frac{1}{2} - \beta$ for $T > 0$. If $\beta < -\frac{1}{2}$, the Airy pulse at $T < 0$ and $T > 0$ accelerates along the negative and positive directions, giving rise to the phenomenon of pulse self-splitting. In the case of $-\frac{1}{2} < \beta < \frac{1}{2}$, the whole pulse accelerates along the positive direction but with different accelerations at $T < 0$ and $T > 0$, respectively. The case of $\beta > \frac{1}{2}$ is opposite to that of $\beta < -\frac{1}{2}$. The corresponding frequency shift is thus given by

$$\delta\omega(Z) = \pm\beta Z. \quad (9)$$

Therefore the spectrum will also exhibit the self-splitting effect with two slopes of $\pm\beta/(2\pi)$, respectively. In addition,

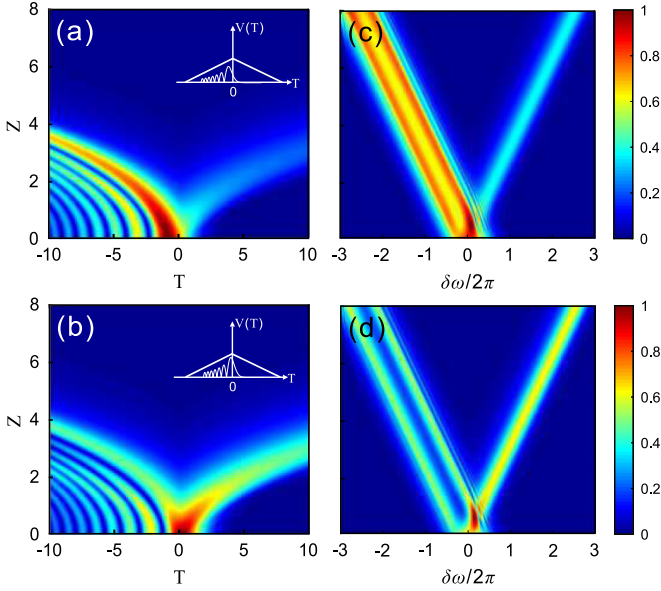


FIG. 3. Temporal evolutions of a finite-energy Airy pulse in a triangle potential with different relative time delay ΔT between the Airy pulse and optical potential with $\beta = -2, a = 0.05$, and $T_0 = 100$ ps. (a) $\Delta T = 0$ and (b) $\Delta T = 1$. (c), (d) The corresponding spectral evolutions in (a), (b), respectively.

the power distribution ratio can be controlled by changing the relative time delay ΔT between the pulse and the potential in both the temporal and spectral domains.

In Fig. 3, we display the numerical simulations of Airy pulse evolution in the triangle potential with $\beta = -2$. As shown in Fig. 3(a), the pulse is divided into two parts, each of which accelerates along a parabolic trajectory but in the opposite directions. By introducing a relative time delay of $\Delta T = 1$ as shown in Fig. 3(b), we can increase the power that accelerates along the positive direction. The corresponding spectral evolutions are shown in Figs. 3(c) and 3(d), both of which exhibit the effects of self-splitting. The effects of self-splitting in both temporal and spectral domains can provide opportunities to control the propagation of the Airy pulse, with potential applications in pulse reshaping and signal manipulation.

B. Airy pulse propagation in parabolic potential

In this section, we consider the situation of a parabolic potential,

$$V(T) = \frac{1}{2}\alpha^2 T^2, \quad (10)$$

where α measures the depth of the potential. Such parabolic potential is originally studied in the context of harmonic oscillators both in classical and quantum regimes. In optics, a Gaussian pulse propagating in a parabolic index distribution medium is analogous to the motion of a harmonic oscillator, which oscillates back and forth and follows a cosine trajectory [25,43], and the Gaussian envelope can be maintained during propagation. For an Airy pulse propagating in a temporal

parabolic potential [45], the envelope evolution is given by

$$U(T, Z) = f(T, Z) \int_{-\infty}^{+\infty} [A(t, 0) \exp(ibt^2)] \exp(-iWt) dt, \quad (11)$$

where

$$W = \alpha T \csc(\alpha Z), \quad b = \alpha \cot(\alpha Z)/2, \\ f(T, Z) = \sqrt{-iW/2\pi T} \exp(ibT^2). \quad (12)$$

By using Fourier transformation, we can obtain

$$U(T, Z) = f(T, Z) \sqrt{i\frac{\pi}{b}} \exp\left(\frac{a^3}{3}\right) \text{Ai}\left(\frac{W}{2b} - \frac{1}{16b^2} + i\frac{a}{2b}\right) \\ \times \exp\left[-i\frac{W^2}{4b} - \frac{1}{3}\left(a + \frac{i}{4b}\right)^3\right] \\ \times \exp\left[\left(a + \frac{i}{4b}\right)\left(\frac{W}{2b} - \frac{1}{16b^2} + i\frac{a}{2b}\right)\right]. \quad (13)$$

From Eq. (13), we find that the Airy pulse follows a periodic oscillating trajectory,

$$T = \frac{1}{4\alpha^2} \frac{\sin^2(\alpha Z)}{\cos(\alpha Z)}, \quad (14)$$

with the oscillation period given by

$$D = \frac{2\pi}{|\alpha|}. \quad (15)$$

Therefore the oscillation period is inversely proportional to the depth of the parabolic potential. At $Z = mD$ ($m = 1, 2, \dots$), the Airy pulse can be restored to its initial profile with $U(T, Z) = U(T, 0)$. At $Z = (2m + 1)D/2$, we have $U(T, Z) = U(-T, 0)$; the pulse envelope is inverted and accelerates in the opposite direction. In particular, for $b = 0$ at $Z = (2m + 1)D/4$, we have

$$U\left(T, Z = \frac{2m+1}{4}D\right) = \sqrt{-i\frac{s\alpha}{2b}} \exp(-\alpha a^2 T^2) \\ \times \exp\left[\frac{a^3}{3} + i\frac{s}{3}(\alpha^2 T^2 - 3a^2 \alpha T)\right], \quad (16)$$

where $s = 1$ as m is even and $s = -1$ as m is odd. Differing from a Gaussian pulse which maintains its shape in the entire propagation process, the Airy pulse will experience a phase transition from an Airy profile to the Gaussian shape at the positions of $Z = (2m + 1)D/4$. From the periodic trajectory, we can also obtain the periodic velocity and acceleration of $v = [\tan(\alpha Z)\sec(\alpha Z) + \sin(\alpha Z)]/(4\alpha)$ and $a = [\sec^3(\alpha Z) + \sec(\alpha Z)\tan^2(\alpha Z) + \cos(\alpha Z)]/4$, both of which reach infinity at these phase transition points.

In Fig. 4(a), we perform numerical simulations of the Airy pulse propagation in parabolic potential with $\alpha = 0.5$. The pulse exhibits a periodic oscillation during propagation with the period of $D = 4\pi$. The instantaneous pulse profiles at $Z = 0, D/4, D/2, 3D/4$, and D are shown in Fig. 4(b). The numerical results can agree well with the theoretical analysis.

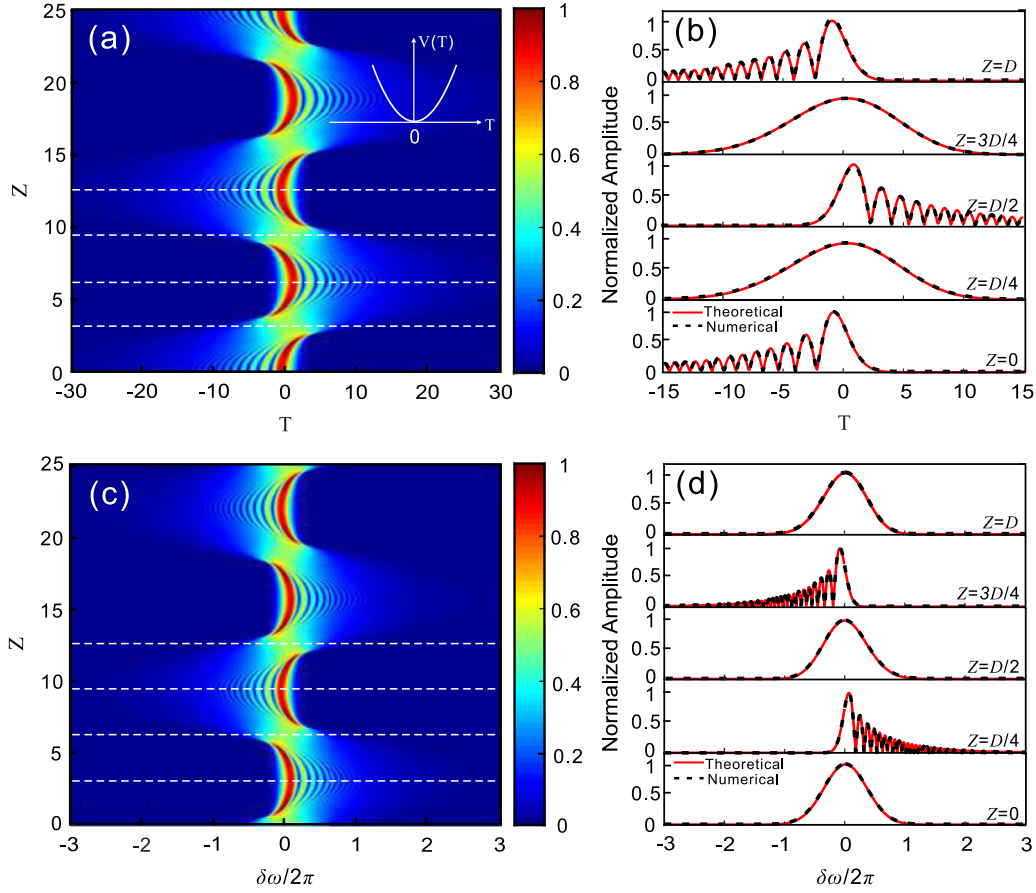


FIG. 4. (a) Temporal evolutions of a finite-energy Airy pulse in parabolic potential with $\alpha = 0.5, a = 0.1$, and $T_0 = 100$ ps. (b) The normalized temporal amplitude profiles at $Z = 0, D/4, D/2, 3D/4$, and D , as marked by the white dashed lines in (a). (c) The spectral dynamics of the Airy pulse corresponding to (a). (d) The normalized amplitude spectra at distances of $Z = 0, D/4, D/2, 3D/4$, and D . The black dashed and red solid lines in (b), (d) represent the numerical and theoretical results, respectively.

It clearly shows that at $Z = D/4$ and $3D/4$, the Airy envelope transforms into a Gaussian profile, which also validates the above analysis.

Figure 4(c) shows the spectral dynamics of an Airy pulse, which is obtained by performing Fourier transformation of the temporal evolution in Fig. 4(a). Of particular interest is that the Gaussian spectrum of the Airy pulse also follows a periodic variation during propagation. The theoretical and numerical spectra features at $Z = 0, D/4, D/2, 3D/4$, and D are shown in Fig. 4(d), which also agree well with each other. At the phase transition points of $Z = D/4$ and $3D/4$, the Gaussian spectrum will transform into an Airy profile, which exhibits a process opposite to that of the temporal evolution.

Now we discuss the influence of potential depth α on the Airy pulse evolution. The pulse center T_C and duration W are defined by the first- and second-order moments of the pulse temporal waveform, respectively [46]:

$$T_C = \frac{\int_{-\infty}^{+\infty} T |U|^2 dT}{\int_{-\infty}^{+\infty} |U|^2 dT}, \quad (17a)$$

$$W = \sqrt{\frac{2 \int_{-\infty}^{+\infty} (T - T_C)^2 |U|^2 dT}{\int_{-\infty}^{+\infty} |U|^2 dT}}. \quad (17b)$$

Analogously, the spectral center and bandwidth can be defined by

$$\omega_C = \frac{\int_{-\infty}^{+\infty} \omega |\tilde{U}|^2 d\omega}{\int_{-\infty}^{+\infty} |\tilde{U}|^2 d\omega}, \quad (18a)$$

$$\Delta\omega = \sqrt{\frac{2 \int_{-\infty}^{+\infty} (\omega - \omega_C)^2 |\tilde{U}|^2 d\omega}{\int_{-\infty}^{+\infty} |\tilde{U}|^2 d\omega}}. \quad (18b)$$

The pulse center shifts during propagation for different α are illustrated in Fig. 5(a), which can be precisely described by Eq. (15). Here the potential depth only changes the oscillation period but has no effect on the maximum shift of the pulse center. The corresponding duration variations for $\alpha = 0.3, 0.5$, and 1 are shown in Fig. 5(b). As α is small [inset in Fig. 5(b)], the potential is very weak and the pulse width experiences considerable expansion during propagation, which is close to the situation of potential-free propagation. For $\alpha = 0.3$, the pulse width reaches the maximum at phase transition points and the minimum at integer multiples of the half oscillation period, while for sufficiently large depth such as $\alpha = 1$, the pulse is squeezed firstly and then broadened, and oscillates with the period of $D/2$.

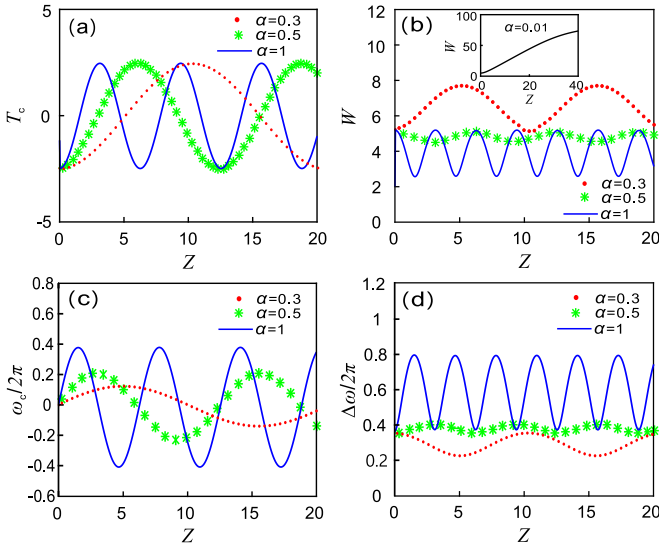


FIG. 5. (a) The center and (b) duration variations of a finite energy Airy pulse during propagation for different depths α . The inset in (b) represents the pulse-width variation as $\alpha = 0.01$. (c), (d) The corresponding spectral center and bandwidth evolutions versus the propagation distance.

Next we turn to the spectral evolution of an Airy pulse in a parabolic potential. Figure 5(c) shows the shifts of the spectral center ω_c as $\alpha = 0.3, 0.5$, and 1, all of which exhibit periodic behaviors; it returns to its initial value at half integer multiples of the oscillation period. The corresponding spectral bandwidth variations $\Delta\omega$ are plotted in Fig. 5(d); the bandwidth is also squeezed and broadened periodically. Note that here the pulse width and spectral bandwidth vary

oppositely, which is basically governed by the uncertainly principle.

C. Airy pulse propagation in higher-order power-law potentials

In this section, we investigate the Airy pulse propagation in higher-order power-law potentials with $n > 2$. The situation is analogous to the propagation of a localized quantum wave packet in an infinite well, which can exhibit periodic revival and antirevival behaviors [43]. Such revival properties can be described by the normalized autocorrelation and anticorrelation functions, which are defined by

$$\begin{aligned} A(Z) &= \int_{-\infty}^{+\infty} U^*(T, Z)U(T, 0)dT \\ &= \int_{-\infty}^{+\infty} \tilde{U}^*(\omega, Z)\tilde{U}(\omega, 0)d\omega, \\ \tilde{A}(Z) &= \int_{-\infty}^{+\infty} U^*(-T, Z)U(T, 0)dT \\ &= \int_{-\infty}^{+\infty} \tilde{U}^*(-\omega, Z)\tilde{U}(\omega, 0)d\omega, \end{aligned} \quad (19)$$

where $U(T, Z)$ and $U(T, 0)$ are the instantaneous and initial temporal wave functions with $\tilde{U}(\omega, Z)$ and $\tilde{U}(\omega, 0)$ being the corresponding amplitude spectra, respectively. $A(Z)$ varies periodically with Z and reaches $|A(Z)| = 1$ at $Z = mZ_T (m = 1, 2, \dots)$, where Z_T is the revival period for the wave packet. At the revival positions, both the temporal and spectral wave packets satisfy $|U(T, mZ_T)| = |U(T, 0)|$ and $|\tilde{U}(\omega, mZ_T)| = |\tilde{U}(\omega, 0)|$. On the contrary, $|\tilde{A}(Z)| = 1$ at the positions of $Z = (m + \frac{1}{2})Z_T (m = 0, 1, \dots)$; both the temporal

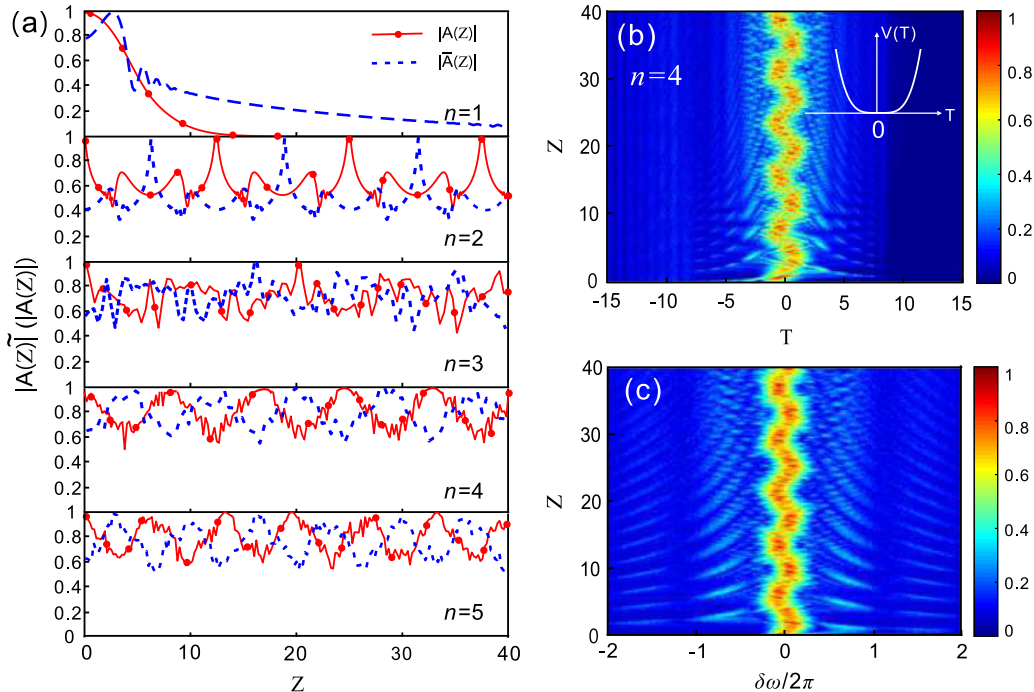


FIG. 6. (a) Normalized autocorrelation (dotted solid red curves) and anticorrelation (dashed blue curves) functions of Airy pulse versus propagation distance in the case of $n = 1, 2, 3, 4$, and 5. (b) Temporal evolutions for the Airy pulse by choosing $n = 4$. (c) The spectral dynamics corresponding to (b). Other parameters are chosen as $\alpha = 0.1, T_0 = 100$ ps, and $V_0 = 0.1$.

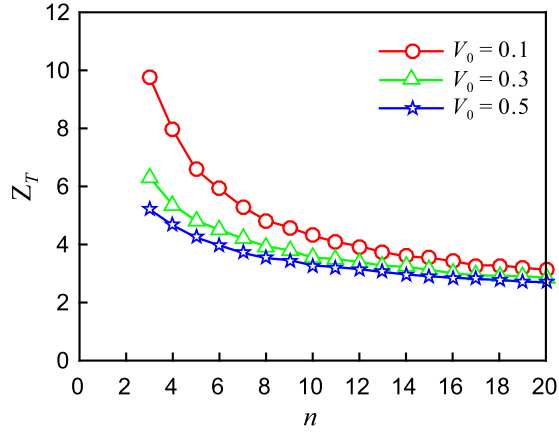


FIG. 7. The revival period of a finite-energy Airy pulse for different potential orders n and depths V_0 . In all cases, we choose $a = 0.1$ and $T_0 = 100$ ps.

waveform and frequency spectrum exhibit mirror symmetries with the initial ones, which satisfy $|U(T, (m + \frac{1}{2})Z_T)| = |U(-T, 0)|$ and $|\tilde{U}(\omega, (m + \frac{1}{2})Z_T)| = |\tilde{U}(-\omega, 0)|$.

In Fig. 6(a), we plot the autocorrelation and anticorrelation functions for $n = 1, 2, 3, 4$, and 5. $A(Z)$ and $\tilde{A}(Z)$ manifest periodic variations and reach the maximum values of 1 at even and odd integer multiples of the half revival period, respectively. Specifically for a linear potential with $n = 1$ as

discussed in Figs. 2 and 3, both $A(Z)$ and $\tilde{A}(Z)$ decrease with Z and ultimately approach 0. The Airy pulse is accelerating all the way without exhibiting either revival or antirevival behaviors. For $n = 2$, both periodic revival and antirevival behaviors of the Airy pulse have been displayed in Fig. 4, which agrees well with the theoretical analysis. Figures 6(b) and 6(c) show the temporal and spectral evolutions of the Airy pulse in the power-law potentials where we choose $n = 4$ as an example. The pulse can be sufficiently localized in the potential well, which experiences periodic oscillations in both the temporal and spectral domains. In Fig. 7, we extract the revival period from the autofunctions of Fig. 6(a) by choosing different potential orders and depths. For a fixed potential depth V_0 , the revival period decreases as n increases, which approaches that of an infinite-depth potential well, while for a fixed potential order n , the revival period can be squeezed by choosing a deeper potential well.

To quantitatively analyze the Airy pulse evolution in a higher-order power-law potential, we examine the variations of the wave-packet center and width for different orders both in time and frequency domains, as defined in Eqs. (17) and (18). Figure 8(a) illustrates the averaged maximum and minimum delay of the pulse center for varying n within the propagation distance $Z = 40$, both of which decrease as n increases, indicating that the wave packet can be better localized. The pulse center distributions for $n = 4$ and 6 are plotted as the inset

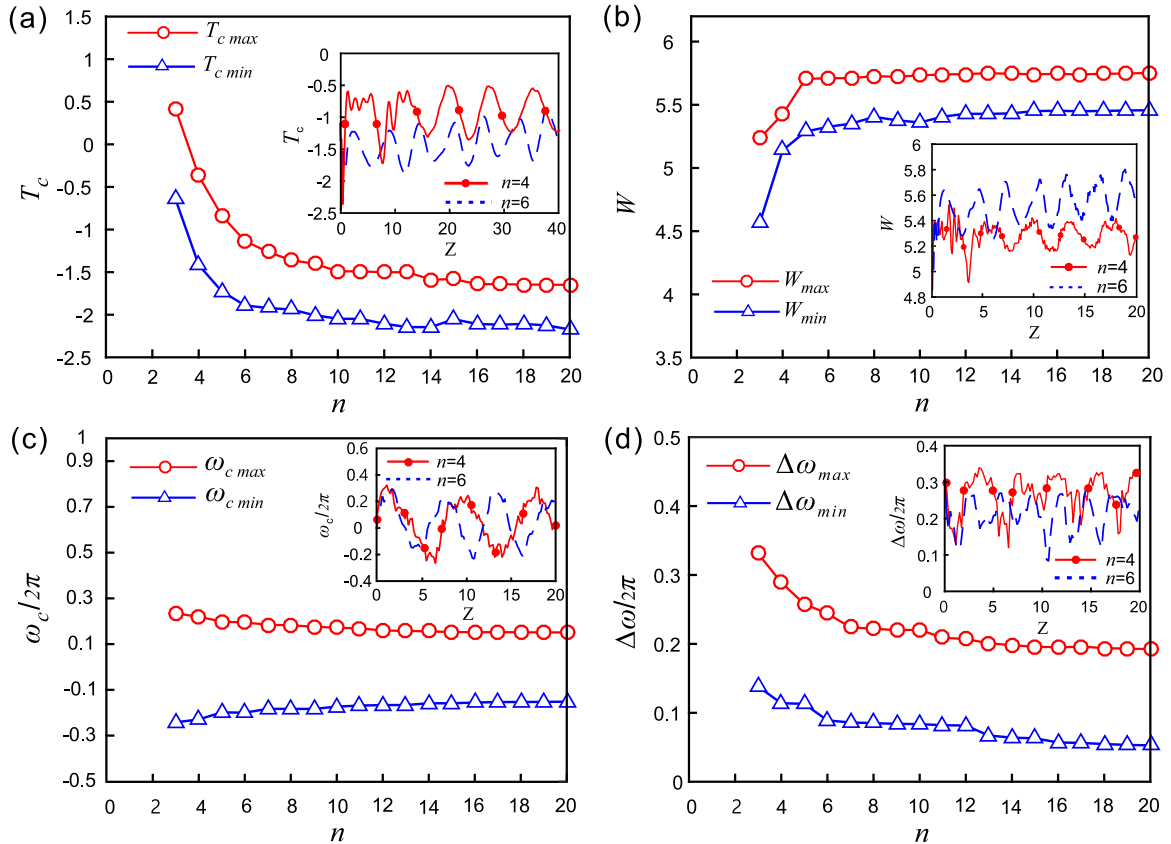


FIG. 8. (a), (b) Averaged maxima and minima of pulse center and duration for different orders n within the propagation distance of $Z = 40$. (c), (d) The corresponding averaged maxima and minima of spectral center and bandwidth versus n . The insets in (a), (b) represent the pulse center and width evolutions with (c), (d) denoting the spectral center and bandwidth evolutions, respectively. Here we choose the orders $n = 4$ and 6. The other parameters are $a = 0.1$, $T_0 = 100$ ps, and $V_0 = 0.1$.

in Fig. 8(a); they oscillate nearly periodically and reach the maximal lateral shifts at antirevival positions. The corresponding pulse-width evolution is shown in Fig. 8(b); it becomes broader as n increases. In addition, the pulse width also varies periodically with the period being half of the pulse center evolution [see the inset in Fig. 8(b)]. It is worth noting that over a longer propagation distance, the pulse will be significantly broadened due to the dispersion; thus $|A(Z)|$ and $|\dot{A}(Z)|$ will decrease with the periodicity becoming weakened gradually.

Next, we display the spectral center and bandwidth of an Airy pulse during propagation for varying orders n . Figure 8(c) shows the averaged frequency shift ω_c for different orders n . The variations of ω_c as $n = 4$ and 6 are also plotted [see the inset in Fig. 8(c)], both of which exhibit periodic behaviors and return to the initial value at half integer multiples of the revival period. Figure 8(d) shows the spectral bandwidth evolution $\Delta\omega$ for different order potentials; it is squeezed as n increases. Since the temporal and spectral wave packets are related to each other through Fourier transformation, their widths vary in opposite ways, accordingly.

IV. CONCLUSIONS

In conclusion, we have investigated the temporal-spectral dynamics of the finite-energy Airy pulse in an optical fiber with

external potentials including linear, parabolic, and higher-order power-law potentials. We find that the acceleration of the Airy pulse can be controlled by changing the gradient of the linear potential, and the corresponding frequency unidirectional shift can be realized. When the linear potential is symmetric, the self-splitting will appear in both temporal and spectral domains during propagation, and power distribution can be controlled by changing the relative delay between the Airy pulse and potential. While in the parabolic potential, the Airy pulse undergoes periodic inversion in both temporal and spectral domains. The pulse also exhibits phase transition points at which an Airy envelope transforms into the Gaussian profile. In addition, the revival and antirevival behaviors are also discussed in higher-order power-law potentials. We find that the revival period decreases as the potential order increases. Our investigation may lead to potential applications in pulse reshaping, temporal-spectral imaging, and signal processing systems.

ACKNOWLEDGMENTS

The work is supported by the 973 Program (Grant No. 2014CB921301), through the National Natural Science Foundation of China (Grant No. 11674117).

-
- [1] M. V. Berry and N. L. Balazs, *Am. J. Phys.* **47**, 264 (1979).
 - [2] G. A. Siviloglou and D. N. Christodoulides, *Opt. Lett.* **32**, 979 (2007).
 - [3] G. A. Siviloglou, J. Broky, A. Dogariu, and D. N. Christodoulides, *Phys. Rev. Lett.* **99**, 213901 (2007).
 - [4] N. K. Efremidis and D. N. Christodoulides, *Opt. Lett.* **23**, 4045 (2010).
 - [5] I. Kaminer, R. Bekenstein, J. Nemirovsky, and M. Segev, *Phys. Rev. Lett.* **108**, 163901 (2012).
 - [6] J. Broky, G. A. Siviloglou, A. Dogariu, and D. N. Christodoulides, *Opt. Express* **16**, 12880 (2008).
 - [7] J. Baumgartl, M. Mazilu, and K. Dholakia, *Nat. Photonics* **2**, 675 (2008).
 - [8] I. Kaminer, M. Segev, and D. N. Christodoulides, *Phys. Rev. Lett.* **106**, 213903 (2011).
 - [9] D. Abdollahpour, S. Suntsov, D. G. Papazoglou, and S. Tzortzakakis, *Phys. Rev. Lett.* **105**, 253901 (2010).
 - [10] A. Chong, W. Renninger, D. N. Christodoulides, and F. W. Wise, *Nat. Photonics* **4**, 103 (2010).
 - [11] P. Polynkin, M. Kolesik, J. V. Moloney, G. A. Siviloglou, and D. N. Christodoulides, *Science* **324**, 229 (2009).
 - [12] A. Minovich, A. E. Klein, N. Janunts, T. Pertsch, D. N. Neshev, and Y. S. Kivshar, *Phys. Rev. Lett.* **107**, 116802 (2011).
 - [13] P. Polynkin, M. Kolesik, and J. Moloney, *Phys. Rev. Lett.* **103**, 123902 (2009).
 - [14] A. Lotti, D. Faccio, A. Couairon, D. G. Papazoglou, P. Panagiotopoulos, D. Abdollahpour, and S. Tzortzakakis, *Phys. Rev. A* **84**, 021807(R) (2011).
 - [15] P. Panagiotopoulos, D. Abdollahpour, A. Lotti, A. Couairon, D. Faccio, D. G. Papazoglou, and S. Tzortzakakis, *Phys. Rev. A* **86**, 013842 (2012).
 - [16] I. Dolev, I. Kaminer, A. Shapira, M. Segev, and A. Arie, *Phys. Rev. Lett.* **108**, 113903 (2012).
 - [17] P. Panagiotopoulos, D. G. Papazoglou, A. Couairon, and S. Tzortzakakis, *Nat. Commun.* **4**, 2622 (2013).
 - [18] A. D. Koulouklidis, D. G. Papazoglou, V. Y. Fedorov, and S. Tzortzakakis, *Phys. Rev. Lett.* **119**, 223901 (2017).
 - [19] C. Ruiz-Jimenez, K. Z. Nobrega, and M. A. Porras, *Opt. Express* **23**, 8918 (2015).
 - [20] Z. Ye, S. Liu, C. Lou, P. Zhang, Y. Hu, D. Song, J. Zhao, and Z. Chen, *Opt. Lett.* **36**, 3230 (2011).
 - [21] X. Huang, Z. Deng, and X. Fu, *J. Opt. Soc. Am. B* **34**, 976 (2017).
 - [22] N. K. Efremidis, *Opt. Lett.* **36**, 3006 (2011).
 - [23] F. Xiao, B. Li, M. Wang, W. Zhu, P. Zhang, S. Liu, M. Premaratne, and J. Zhao, *Opt. Express* **22**, 22763 (2014).
 - [24] Y. Zhang, M. R. Belić, L. Zhang, W. Zhong, D. Zhu, R. Wang, and Y. Zhang, *Opt. Express* **23**, 10467 (2015).
 - [25] Y. Zhang, X. Liu, M. R. Belić, W. Zhong, M. S. Petrović, and Y. Zhang, *Ann. Phys.* **363**, 305 (2015).
 - [26] G. P. Agrawal, *Nonlinear Fiber Optics* (Academic Press, New York, 2013).
 - [27] M. Miyagi and S. Nishida, *Appl. Opt.* **18**, 678 (1979).
 - [28] C. Chang, H. P. Sardesai, and A. M. Weiner, *Opt. Lett.* **23**, 283 (1998).
 - [29] I. M. Besieris and A. M. Shaarawi, *Phys. Rev. E* **78**, 046605 (2008).
 - [30] C. Ament, P. Polynkin, and J. V. Moloney, *Phys. Rev. Lett.* **107**, 243901 (2011).
 - [31] L. Zhang, H. Zhong, Y. Li, and D. Fan, *Opt. Express* **22**, 22598 (2014).
 - [32] L. Zhang, J. Zhang, Y. Chen, A. Liu, and G. Liu, *J. Opt. Soc. Am. B* **4**, 889 (2014).

- [33] X. Shi, C. Tan, Y. Bai, R. Wang, Z. Zhang, and X. Fu, *J. Opt. Soc. Am. B* **9**, 1816 (2015).
- [34] R. Driben, Y. Hu, Z. Chen, B. A. Malomed, and R. Morandotti, *Opt. Lett.* **38**, 2499 (2013).
- [35] S. Wang, D. Fan, X. Bai, and X. Zeng, *Phys. Rev. A* **89**, 023802 (2014).
- [36] L. Zhang, K. Liu, H. Zhong, J. Zhang, Y. Li, and D. Fan, *Opt. Express* **23**, 2566 (2015).
- [37] Y. Fattal, A. Rudnick, and D. M. Marom, *Opt. Express* **19**, 17298 (2011).
- [38] X. Zhong, X. Du, and K. Cheng, *Opt. Express* **23**, 029467 (2015).
- [39] C. Bersch, G. Onishchukov, and U. Peschel, *Appl. Phys. B* **104**, 495 (2011).
- [40] A. Bell, K. Wang, S. Solntsev, N. Neshev, A. Sukhorukov, and J. Eggleton, *Optica* **4**, 1433 (2017).
- [41] C. Qin, F. Zhou, Y. Peng, D. Sounas, X. Zhu, B. Wang, J. Dong, X. Zhang, A. Alù, and P. Lu, *Phys. Rev. Lett.* **120**, 133901 (2018).
- [42] F. Wang, S. Ke, C. Qin, B. Wang, H. Long, K. Wang, and P. Lu, *Optics and Laser Technology* **103**, 272 (2018).
- [43] R. W. Robinett, *Phys. Rep.* **392**, 1 (2004).
- [44] F. Gori, M. Santarsiero, R. Borghi, and G. Guattari, *Eur. J. Phys.* **20**, 477 (1999).
- [45] C. Bernardini, F. Gori, and M. Santarsiero, *Eur. J. Phys.* **16**, 58 (1995).
- [46] I. M. Besieris and A. M. Shaarawi, *Opt. Lett.* **32**, 2447 (2007).